Article:
Steinschulte, AA, Scotti, A, Rahimi, K et al. (2017) Stimulated Transitions of Directed Nonequilibrium Self-Assemblies. Advanced Materials, 29 (43). 1703495. ISSN: 0935-9648

https://doi.org/10.1002/adma.201703495

DOI: 10.1002/((please add manuscript number))
Article type: Communication

Stimulated Transitions of Directed Non-Equilibrium Self-Assemblies

Alexander A. Steinschulte, Andrea Scotti, Khosrow Rahimi, Oleksii Nevskyi, Alex Oppermann, Sabine Schneider, Steffen Bochenek, Marie F. Schulte, Karen Geisel, Felicitas Jansen, Andre Jung, Sabrina Mallmann, Roland Winter, Walter Richtering, Dominik Wöll, Ralf Schweins, Nicholas J. Warren, Felix A. Plamper**

A. A. Steinschulte, Dr. A. Scotti, O. Nevskyi, A. Oppermann, S. Schneider, S. Bochenek, M. Schulte, Dr. K. Geisel, F. Jansen, A. Jung, Prof. W. Richtering. Prof. D. Wöll, F. A. Plamper
Institute of Physical Chemistry, RWTH Aachen University, Landoltweg 2, D-52056 Aachen, Germany.
E-mail: plamper@pc.rwth-aachen.de

S. Mallmann, Dr. K. Rahimi
DWI Leibniz Institute for Interactive Materials and Center for Chemical Polymer Technology (CPT) Forckenbeckstr. 50, D-52074 Aachen, Germany.

Prof. R. Winter
Department of Chemistry and Chemical Biology, Physical Chemistry I, TU Dortmund University, Otto-Hahn Str. 6, D-44227 Dortmund, Germany.

Dr. R. Schweins
Institut Laue-Langevin ILL, DS/LSS, 71 Avenue des Martyrs, F-38000 Grenoble, France.
Department of Chemistry, University of Sheffield, Brook Hill, Sheffield, South Yorkshire S3 7HF, UK.

Dr. N. J. Warren
School of Chemical and Process Engineering, University of Leeds, Leeds LS2 9JT, UK.
E-mail: n.warren@leeds.ac.uk

Keywords: micelles, hydrostatic pressure, small angle neutron scattering, rheology, gels

ABSTRACT: Near-equilibrium stimuli-sensitive polymers have been used extensively to introduce morphological variations in dependence of adaptable conditions. Far less well studied are triggered transformations at constant conditions. These require the involvement of metastable states, which are either able to approach the equilibrium state after deviation from metastability or can be frozen on returning from non-equilibrium to equilibrium. Such functional non-equilibrium macromolecular systems hold great promise for on-demand

transformations, which result in substantial changes in their material properties, as seen for triggered gelations. Herein, we introduce a diblock copolymer system consisting of a hydrophilic block and a block, which is responsive to both pressure and temperature. This species demonstrates various micellar transformations, upon leaving equilibrium/non-equilibrium states, which are triggered by a temperature deflection or a temporary application of hydrostatic pressure.

MAIN TEXT:

Biological systems consist of soft-matter in a non-equilibrium state, and is as such regarded as a prerequisite for sustaining life on earth. Consequently, future advances in fields such as synthetic biology will require the ability to accurately reproduce non-equilibrium self-assembled soft matter systems by tuning the delicate balance between numerous kinetic parameters.[1] Failures in this field often occur due to kinetic trapping on the pathway toward these structures. Hence, soft matter research has mainly focused on equilibrium morphologies, including block copolymer self-assembly, which provides well-defined nanostructures.[2, 3] These range from unimolecular,[4] conventional spherical micelles,[5] worms,[6] lamellae[7] to vesicles[8]. The thermodynamic aspects are well understood from a theoretical point of view[9, 10] and certain methods have been employed to approach the equilibrium state experimentally, such as solvent exchange from a common to a selective solvent[2] or thin-film rehydration.[5] Colloidal structures, which bear resemblance to naturally occurring systems, can be prepared reproducibly in the laboratory during synthesis.[11, 12] Polymerization-Induced Self-Assembly (PISA)[13] is an example of a technique which can produce nanostructures in an extremely predictable manner. This utilizes precise control afforded by the Reversible Addition Fragmentation Transfer (RAFT)[14] dispersion polymerization with the help of a soluble polymeric chain transfer agent (macro-CTA).

Despite these advances, the benefits of non-equilibrium micellar arrangements have only recently been addressed, including their morphological versatility (access to morphologies that are otherwise not available from a thermodynamic point of view).[15] The processing of such assemblies can determine their final structure.[16] A less regarded feature of non-equilibrium morphologies is the triggered transition from a local minimum (metastable or frozen state) toward the global minimum of the free energy landscape.[1, 17] Alternatively, temporary deflections from the global minimum and intermediate structural freezing in a metastable state could also be used for stimulated transitions. These, often miniscule deflections from the energy minimum could present opportunities for novel nanostructures, allowing considerable changes in the properties which surpass the abilities of known responsive materials.[18] Application of a (local) trigger (e.g. subtle temperature variation) can lead to far-reaching global structural transformations. However, such triggered soft matter transitions are fairly unexplored, though other kinetic aspects have already been addressed (like a time-programmed switching[19] or a control of hierarchically organized materials by sequenced insolubility-adjustment of different blocks of terpolymers[20]). Here, we will use local minima in the energy landscape to switch between desired material properties at constant conditions. We make use of stimuli-responsive polymers to enhance the transitional restructuring dynamics due to temporary solubilization.

Poly(*N*-isopropyl acrylamide) (PNIPAM) is a known temperature-responsive polymer,[21] which is well hydrated below its lower critical solution temperature (LCST at 32°C). Polymerizing NIPAM [22] in the presence of a soluble poly(dimethyl acrylamide) (PDMAM) macro-CTA, results in diblock copolymers which undergo spontaneous self-assembly due to the segregated[23] PNIPAM component (when synthesis conducted above LCST).[24] Unfortunately, these nano-objects could not conveniently be studied in a non-equilibrium state as the PNIPAM required crosslinking to avoid unimolecular dissolution at ambient temperature. Fortunately, by copolymerizing NIPAM with *tert*-butyl acrylamide (tBAM), the

LCST of the resulting copolymer can be reduced below ambient temperature.[25] This effect of hydrophobic comonomers on the polymer transition temperature is well captured also in a simulation or theory context.[26]

Besides its thermosensitivity, the response of PNIPAM to pressure is often overlooked:[27] precipitated (> LCST) PNIPAM can be re-solvated by increasing pressure.[28] Theoretically, this effect can be explained by the pressure-induced decrease of the volume of the solvent-inaccessible cavities, which are formed by hydrophobic interactions.[29] This study also demonstrates that pressure and temperature act antagonistically. Beneficially, hydrostatic pressure can be applied and released more rapidly than temperature variations, pressure propagates uniformly and can be readily applied bidirectionally, i.e. during pressurization and depressurization. In addition, pressure effects are ubiquitous and extend into fields like mining, geology, oil recovery (fracking) and deep-sea biology. Considerable pressure variations are even encountered in biological tissues (e.g. joints upon impact/jumping).[29]

Herein, we demonstrate a directed formation of various diblock terpolymer nanostructures in water by tuning the solid content and the length of the insoluble 'core-forming' block. Most importantly, we demonstrate a pathway for the directed preparation of both equilibrium and non-equilibrium structures for individual copolymer compositions using three different techniques: (a) Tuning the polymerization conditions and possible subsequent concentration adaption, (b) applying temperature *and/or* (c) pressure triggers. Furthermore, it is possible to choose between reversible (via all-equilibrium or near-equilibrium pathways) and irreversible morphology changes (to/from equilibrium including further possible intermediate non-equilibrium situations), when returning to the starting conditions. These systems are probed by small-angle neutron scattering (SANS), transmission electron microscopy (TEM), cryogenic scanning electron microscopy (cryo-SEM), superresolution fluorescence microscopy and oscillatory rheology.

A facile RAFT aqueous polymerization system (**Figure 1**A) is utilized to synthesize equilibrium/non-equilibrium structures by simply changing the polymerization formulation. PISA was conducted with a statistical copolymerization of NIPAM and tBAM in the presence of a water-soluble poly(*N*,*N*-dimethylacrylamide) $PDMAM_{49}$ macro-CTA (index assigns degree of polymerization *DP*). The mol% of tBAM in the core was maintained at 35 % in order to keep the LCST below room temperature (see Figure S1).

In all reactions, all monomer was consumed within 2 hours (Figure S2), resulting in low dispersity $PDMAM_{49}$-*b*-P(NIPAM-*st*-tBAM)$_{DP}$ copolymers (Figure S3). The predictable nature of PISA enabled reproducible synthesis of multiple morphologies (spheres, worms and vesicles) allowing a 'phase diagram' to be constructed (Figure S4).

To investigate the equilibrium behavior of this formulation, the 'phase diagram' was used to select $PDMAM_{49}$-*b*-P(NIPAM-*st*-tBAM)$_{DP}$ samples synthesized at high concentration (200 g/L; abbreviated A_{49}-*b*-B_{DP}HSC) and samples with equivalent copolymer composition obtained at low synthesis concentration (50 g/L; abbreviated as A_{49}-*b*-B_{DP}LSC). At high concentrations equilibrium spheres (**IV**), worms (**V**) and unilamellar vesicles (**VI**) were readily accessed by increasing *DP*.[13] This sequence is in line with the sequence of equilibrium morphologies as seen by theory,[10, 30] which is based on a detailed analysis of core, interface and corona contributions to the free energy, showing that star-like micelles are preferred with short solvophobic blocks (compared to solvophilic blocks), whereas vesicles are thermodynamically stable with long solvophobic blocks. In between, a narrow phase region with worm-like micelles is predicted. Presence of mixed phases (see Figure S4) containing e.g. spheres/worms or worms/vesicles close to the respective phase boundary does not contradict theory. Hence, the synthesis at high concentration allows access to all these (equilibrium) structures. For reasons discussed below,[32] low concentration synthesis produced only spherical micelles with increasing diameter (**I-III)** for all compositions (see Figure 1B) implying non-equilibrium for larger spheres.[6, 12]

First, we regard reversible transitions. E.g. temperature dependent SANS[31] studies on the A_{49}-*b*-B_{50}LSC small spherical micelles indicate the presence of core-corona structures (**I**) at 25°C followed by molecular dissolution on cooling. On returning to 25°C, the superimposable SANS patterns indicate a fully reversible transition (see **Figure 2** A, B and Figure S5), illustrating their equilibrium character.[32]

The A_{49}-*b*-B_{90}HSC worm-like micelles (**V**) are present in a narrow *DP* range (see Fig S4). These worms are observed in post-mortem TEM studies and in the SANS pattern[31], which displays a q^{-1} dependence at low *q* characteristic of worm-like micelles (Figure 2D and E in its diluted state; a pure worm dispersion according to SANS; spherical "impurities" in TEM may have been caused by drying).[32] Furthermore, the presence of worms is suggested by the formation of a strong freestanding gel. [33] The exact length of the worms is not accessible by SANS, due to the limited available *q*-range. [32] The 'as synthesized' A_{49}-*b*-B_{90}HSC dispersion of this copolymer also displays fully reversible (de)gelation, with a change in storage modulus (G') over three orders of magnitude due to the dissolution of the worm-like micelles (Figure 2F). These observations are in accordance with other studies on cylindrical or worm-like micelles, [33] and indicate that the worm-like micelles represent probably the 'equilibrium' morphology.

Subtle conditions for the equilibrium/non-equilibrium adjustment are present in this system, as seen in the concentration effect for the same polymer. Sample **II(&III)** are likely to be non-equilibrium kinetically-trapped structures, and are referred to as 'crew-cut' micelles. [10] In these systems, it was shown that they maintained their kinetically trapped morphology for >1 year at ambient temperature.

As a first example for non-equilibrium transitions, A_{49}-*b*-B_{90}LSC with the same composition as the worm-sample above (Figure 2C-F; DP=90) forms spherical micelles (**II**) in a dilute synthesis. However, a remarkable decrease in the A_{49}-*b*-B_{90}LSC core radius is observed,[32] when conducting a temperature cycle (see **Figure 3** and Figure S5). This means, that despite

being the same spherical morphology, both micelle-types are probably in a non-equilibrium state (crew-cut), as reversible cylindrical micelles were observed with the same composition (see Figure 2). Furthermore, A_{49}-*b*-B_{90}LSC which was concentrated by freeze-drying and dissolving in cold water also forms a free-standing gel, similar as A_{49}-*b*-B_{90}HSC (see Figure S8). All these observations suggest that the concentration is a critical factor affecting the formation of worms both during PISA *and* during the temperature-induced self-assembly. Additionally, differences in morphology evolution arise due to the presence of monomer during PISA, which plasticizes the glassy PNIPAM domain, especially at high solid content.[32]

A further intriguing morphological transition occurs for the samples with longer *DP* upon experiencing the temperature cycle. When targeting a longer core *DP* of 400, the concentration effect is seen once more; on this occasion, vesicles (**VI**) are formed during PISA at high concentration, while crew-cut (**III**) micelles are seen at low concentrations.

The vesicles (**VI**) remain stable upon dilution to low concentration resulting in two different micellar morphologies (**III**&**VI**) under the same conditions (left side **Figure 4**). Due to the non-equilibrium state of at least one of the structures, there is a thermodynamic driving force toward the equilibrium structure upon application of a trigger (see Figure 3). This includes further trapping on this pathway, as the equilibrium structure for A_{49}-*b*-B_{400} is likely in the vesicular state, which cannot be recovered after triggering. More specifically, both samples (**III**&**VI**) dissociate when cooled, forming dissolved chains. On warming, they undergo a dissolved chains>sphere>worm transition (Figure 3). This is associated with an increase in viscosity. Although the initial morphology is different, these two samples therefore broadly show the same transitions in both the SANS and the rheology experiments, when subjected to the same temperature cycle.

Hence we extend Figure 4 by the triggered structures, demonstrating a very rare example of a single composition present as spherical micelles, worm-like micelles and vesicles under the

same conditions (solvent, pH, temperature, pressure). The resulting worm-like micelles are physically interconnected and cannot be diluted in water (in contrast to the reversible worms; Figure 2C-F). Hence, not only the material properties of the gels can be programmed at the synthesis stage, but also the gelation can be decoupled from the polymerization, allowing triggered gel formation without further chemistry.

SANS can also provide an insight into these transitions. The patterns for A_{49}-*b*-B_{400}LSC (**III**) at 25 °C and 15 °C (during cooling) are in line with a crew-cut structure, fitting a hard sphere model incorporating a repulsive structure factor (required due to high concentration).[32] At 5 °C, the majority of the spherical micelles dissociate into unimolecularly dissolved polymer. When the temperature is increased to 15 °C, the scattering pattern changes drastically compared to the one at 15 °C before cooling. Upon further heating, the SANS data at 25 °C indicates a sphere-to-worm transition (Figure 3D).[32] On large scale, the worm-like micelles form an interconnected porous network, visualized in the cryo-SEM (Figure 3F) and superresolution fluorescence microscopy (Figure S11). From SANS experiments, we do not obtain information about the formed interconnected network, due to the limited *q*-range. The cylindrical model, which fits reasonably well to the scattering data, is only appropriate for the observed *q*-range.

The behavior of the diluted A_{49}-*b*-B_{400}-HSC vesicles (**VI**) is comparable to the equivalent crew-cut micelles(**III**). Despite the difference in morphology before conducting a temperature cycle, on cooling they undergo a vesicle-to-unimer transition as observed in the SANS studies (Figure 3G and H).[32] This observation is unsurprising given that the two samples consist of polymers with near identical composition and concentration. Furthermore, there is no intermediate worm-phase during this transition, which might be expected.

Variable frequency rheology measurements conducted at 25°C show that both the crew-cut (**III**) and vesicular micelles (**VI**) behave as a viscoelastic fluid, (Figure S9) with G' and G" values around 10^{-1} Pa (at 1 Hz), as would be expected for isotropic particles. During the

variable temperature rheology studies (Figure 3E), only subtle changes in rheology were observed on cooling, where a slight increase in the moduli is observed during the sphere-to-unimer transition. On warming, an increase in the moduli occurs and a gel is formed at approximately 7 ºC, whereupon the value for G' increases above G" (at 1 Hz). It is noteworthy that there is a plateau in gel modulus at intermediate temperatures (around 15 °C) which is followed by a second increase at 23 °C. The first plateau can be attributed to a gel formed by the high volume fraction of the small repulsive spheres which were also observed in the SANS measurements at 15 °C (formation of a colloidal glass). The second plateau with high viscosity is formed by the cylindrical micelles, which form a porous network, visualized in the cryo-SEM (Figure 3F & J). This network forms an interconnected free-standing gel (G' $\approx 10^3$ Pa), also confirmed by the tube inversion test (see digital images in Figure 3). Due to the interconnection, it is not possible to further dilute this network. As a consequence, the gel is stable against an excess of water. A second temperature cycle shows that any subsequent gel formation / dissolution (at low temperature) is again reversible (see Figure S10).

Although convenient, using a temperature trigger often lacks rapid implementation, as heating and cooling are slow. Hydrostatic pressure is an alternative trigger,[34] which is much faster, only limited by the speed of sound (μs timescale). An interesting property of PNIPAM polymers, is the ability to use pressure as a stimulus. The present system enables a direct comparison of pressure and temperature stimuli. Moreover, the ability to conduct variable pressure SANS studies enables direct observation of morphology changes.

The hydrostatic pressure was increased at a constant temperature of 15 °C. Up to 400 bar, the scattering does not change considerably (see Figures S12 for all measurements), but increasing to 800/1000 bar the data can be fitted to a Gaussian coil model, suggesting complete dissolution. Upon decompression, rapid re-micellization occurs, with the final pattern upon return to ambient pressure (at 15 °C) resembling that obtained at 15 °C after applying a temperature trigger (see **Figure 5** and 3).

For A_{49}-*b*-B_{90}LSC, crew-cut micelles (**II**) re-assemble to smaller spheres upon intermediate pressure application, resembling very much the temperature-triggered transition.[32] For A_{49}-*b*-B_{400}LSC (**III**) and diluted A_{49}-*b*-B_{400}HSC (**VI**), a q^{-1} dependency is observed after subsequent heating to 25 °C, analogous to the measurement at 25 °C after the temperature trigger.[32] Again, the data is consistent with the transition to worm-like micelles driven by the pressure deflection (for cryo-SEM see Figure S13).[32] The striking similarities between pressure and temperature cycles reveal that pressure acts as a facile trigger for the rearrangement of the micelles, including irreversible structural transitions toward small spherical and then finally worm-like micelles.

In conclusion, we demonstrate that NIPAM-containing amphiphilic block copolymers, obtained by RAFT aqueous dispersion polymerization, self-assemble into different nanostructures with high fidelity due to a polymerization-induced self-assembly. By just adjusting the *DP* of the core-forming block and the concentration during preparation, one can choose between non-equilibrated and equilibrated samples. At low concentrations, the particles formed are spherical micelles. At high concentrations, all morphologies are accessible by varying *DP*.

Reversible changes in morphology are observed for spherical and worm-like micelles near equilibrium, but irreversible morphology changes occur for a longer *DP* of 400 regardless of the initial morphology: both crew-cut micelles and vesicles undergo order-disorder transitions on cooling, forming freely soluble chains. But on returning to the original conditions, they both get trapped in a continuous network of worms.

These morphological transitions result in pronounced changes in physico-chemical properties. For example, fluid samples of low viscosity form free-standing gels after application of the trigger. These examples show that a proper choice of non-equilibrium conditions allows for an on-demand property change. We expect that this research stimulates further studies on general transformations, where not only small temperature and pressure cycles but also other

stimuli (e.g. light) provide sufficient deviations from morphological metastability to induce large property changes. In addition, "rechargeable" micellar systems would allow the use of the same polymer for several subsequent non-equilibrium micellar transformations. In all, this will advance the benefits of non-equilibrium matter for a variety of applications (e.g. biomedical), where on-demand gelation occurs without chemical modification. Like a spark,[35] a marginal trigger can ignite huge changes in the colloidal system along the thermodynamic landscape toward the global free energy minimum.

Supporting Information
Supporting Information is available from the Wiley Online Library or from the author.

Acknowledgements
The authors are indebted to Steve Armes for his introduction to PISA and to Oleg Borisov and Vladimir Aseyev for fruitful discussions. The high pressure group of ILL, especially C. Payre and J. Maurice, is thanked for their help with running the high pressure cell. The funding by the German Research Foundation (DFG, Project PL 571/3-2 and SFB 985 "Functional Microgels and Microgel Systems") is gratefully acknowledged.

Received: ((will be filled in by the editorial staff))
Revised: ((will be filled in by the editorial staff))
Published online: ((will be filled in by the editorial staff))

References

[1] E. Mattia, S. Otto, *Nat. Nanotechnol.* **2015**, *10*, 111.

[2] Y. Mai, A. Eisenberg, *Chem. Soc. Rev.* **2012**, *41*, 5969.

[3] U. Tritschler, S. Pearce, J. Gwyther, G. R. Whittell, I. Manners, *Macromolecules* **2017**, *50*, 3439; A. A. Steinschulte, A. P. H. Gelissen, A. Jung, M. Brugnoni, T. Caumanns, G. Lotze, J. Mayer, D. V. Pergushov, F. A. Plamper, *ACS Macro Lett.* **2017**, 711; C. L. Dähling, G.; Mori, H.; Pergushov, D. V.; Plamper, F. A.,, *J. Phys. Chem. B* **2017**.

[4] A. A. Steinschulte, B. Schulte, M. Erberich, O. V. Borisov, F. A. Plamper, *ACS Macro Lett.* **2012**, *1*, 504.

[5] L. Zhang, A. Eisenberg, *Science* **1995**, *268*, 1728.

[6] A. Blanazs, A. J. Ryan, S. P. Armes, *Macromolecules* **2012**, *45*, 5099.

[7] G. Rizis, T. G. M. van de Ven, A. Eisenberg, *Angew. Chem. Int. Edit.* **2014**, *53*, 9000.

[8] D. E. Discher, A. Eisenberg, *Science* **2002**, *297*, 967.

[9] P. G. de Gennes, *Macromolecules* **1980**, *13*, 1069.

[10] O. V. Borisov, E. B. Zhulina, F. A. M. Leermakers, A. H. E. Müller, in *Self Organized Nanostructures of Amphiphilic Block Copolymers I*, (Eds: E. A. H. Müller, O. Borisov), Springer Berlin Heidelberg, Berlin, Heidelberg 2011, 57.

[11] K. Matyjaszewski, N. V. Tsarevsky, *Nat. Chem.* **2009**, *1*, 276.

[12] S. Sugihara, A. Blanazs, S. P. Armes, A. J. Ryan, A. L. Lewis, *J. Am. Chem. Soc.* **2011**, *133*, 15707.

[13] N. J. Warren, S. P. Armes, *J. Am. Chem. Soc.* **2014**, *136*, 10174.

[14] D. J. Keddie, G. Moad, E. Rizzardo, S. H. Thang, *Macromolecules* **2012**, *45*, 5321.

[15] R. C. Hayward, D. J. Pochan, *Macromolecules* **2010**, *43*, 3577; H. Cui, Z. Chen, S. Zhong, K. L. Wooley, D. J. Pochan, *Science* **2007**, *317*, 647.

[16] Y.-H. Tang, Z. Li, X. Li, M. Deng, G. E. Karniadakis, *Macromolecules* **2016**, *49*, 2895; X. Ye, M. R. Jones, L. B. Frechette, Q. Chen, A. S. Powers, P. Ercius, G. Dunn, G. M. Rotskoff, S. C. Nguyen, V. P. Adiga, A. Zettl, E. Rabani, P. L. Geissler, A. P. Alivisatos, *Science* **2016**, *354*, 874; W. Li, M. Müller, *Prog. Polym. Sci.* **2016**, *54–55*, 47; K. Kim, M. W. Schulze, A. Arora, R. M. Lewis, M. A. Hillmyer, K. D. Dorfman, F. S. Bates, *Science* **2017**, *356*, 520.

[17] S. Mann, *Nat. Mater.* **2009**, *8*, 781.

[18] H. Qiu, Y. Gao, V. A. Du, R. Harniman, M. A. Winnik, I. Manners, *J. Am. Chem. Soc.* **2015**, *137*, 2375; J. R. Lovett, N. J. Warren, S. P. Armes, M. J. Smallridge, R. B. Cracknell,

Macromolecules **2016**, *49*, 1016; N. J. Warren, O. O. Mykhaylyk, D. Mahmood, A. J. Ryan, S. P. Armes, *J. Am. Chem. Soc.* **2014**, *136*, 1023; X. Wang, X. Feng, G. Ma, D. Zhang, Y. Chai, M. Ge, L. Yao, *Adv. Mater.* **2017**, *29*, 1605932; X. Su, P. Wei, H. Li, W. Liu, Y. Yan, P. Li, C. Su, C. Xie, W. Zhao, P. Zhai, Q. Zhang, X. Tang, C. Uher, *Adv. Mater.* **2017**, *29*, 1602013; A. Mourran, H. Zhang, R. Vinokur, M. Möller, *Adv. Mater.* **2017**, *29*, 1604825.

[19] T. Heuser, A.-K. Steppert, C. Molano Lopez, B. Zhu, A. Walther, *Nano Lett.* **2015**, *15*, 2213; T. Heuser, R. Merindol, S. Loescher, A. Klaus, A. Walther, *Adv. Mater.* **2017**, *29*, 1606842.

[20] A. H. Gröschel, A. Walther, T. I. Loebling, F. H. Schacher, H. Schmalz, A. H. E. Müller, *Nature* **2013**, *503*, 247.

[21] A. Halperin, M. Kröger, F. M. Winnik, *Angew. Chem. Int. Edit.* **2015**, *54*, 15342.

[22] Q. Li, C. Gao, S. Li, F. Huo, W. Zhang, *Polym. Chem.* **2014**, *5*, 2961; W. Wang, C. Gao, Y. Qu, Z. Song, W. Zhang, *Macromolecules* **2016**, *49*, 2772.

[23] P. Hebbeker, A. A. Steinschulte, S. Schneider, F. A. Plamper, *Langmuir* **2017**, *33*, 4091.

[24] C. A. Figg, A. Simula, K. A. Gebre, B. S. Tucker, D. M. Haddleton, B. S. Sumerlin, *Chem. Sci.* **2015**, *6*, 1230.

[25] J. D. Debord, L. A. Lyon, *Langmuir* **2003**, *19*, 7662.

[26] B. Schulz, R. Chudoba, J. Heyda, J. Dzubiella, *J. Chem. Phys.* **2015**, *143*, 243119.

[27] S. Grobelny, C. H. Hofmann, M. Erlkamp, F. A. Plamper, W. Richtering, R. Winter, *Soft Matter* **2013**, *9*, 5862.

[28] M. Shibayama, K. Isono, S. Okabe, T. Karino, M. Nagao, *Macromolecules* **2004**, *37*, 2909.

[29] M. Reinhardt, J. Dzubiella, M. Trapp, P. Gutfreund, M. Kreuzer, A. H. Gröschel, A. H. E. Müller, M. Ballauff, R. Steitz, *Macromolecules* **2013**, *46*, 6541.

[30] E. B. Zhulina, O. V. Borisov, *Macromolecules* **2005**, *38*, 6726.

[31] All SANS experiments performed on D11 at ILL Grenoble doi:10.5291/ILL-DATA.9-10-1470.

[32] See Supporting Information

[33] R. Verber, A. Blanazs, S. P. Armes, *Soft Matter* **2012**, *8*, 9915; T. M. Clausen, P. K. Vinson, J. R. Minter, H. T. Davis, Y. Talmon, W. G. Miller, *J. Phys. Chem.* **1992**, *96*, 474.

[34] Y. Liu, J. D. Spring, M. Steinhart, R. Bansil, *Macromolecules* **2012**, *45*, 9147.

[35] L. Cera, L. Chiappisi, C. Böttcher, A. Schulz, S. Schoder, M. Gradzielski, C. A. Schalley, *Adv. Mater.* **2017**, *29*, 1604430

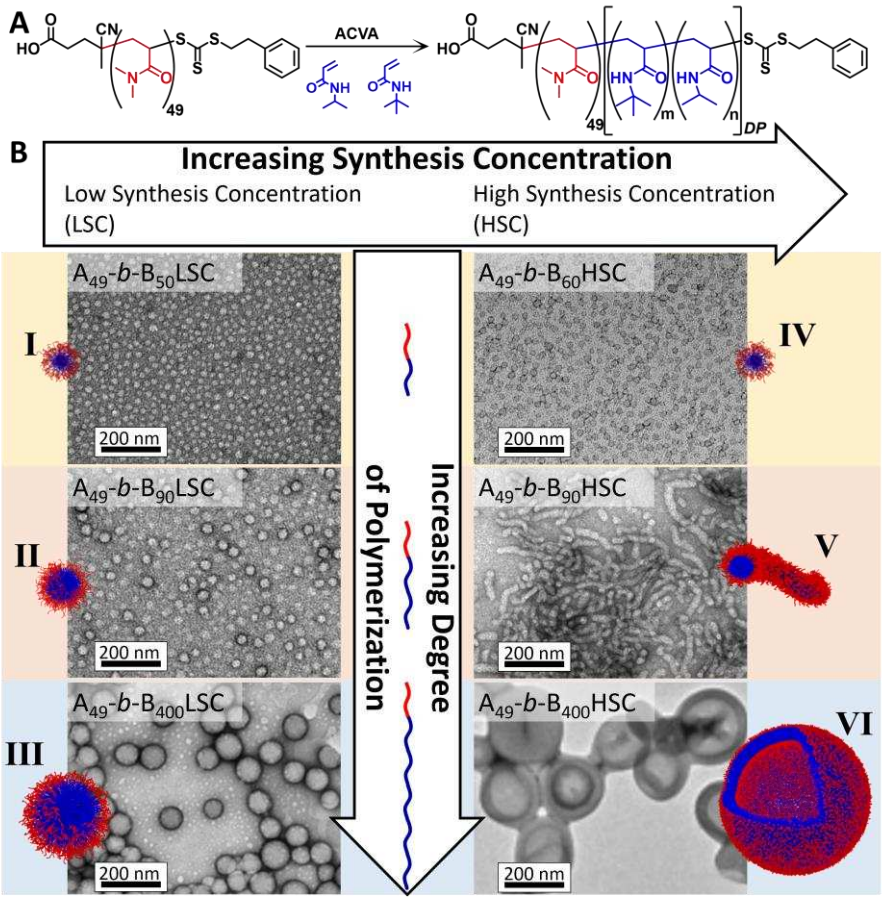

Figure 1. (A) Reaction scheme of the RAFT copolymerization of NIPAM and tBAM at 70 °C in water. (B) Scheme of morphologies including TEM images (negatively stained) of representative PDMAM$_{49}$-*b*-P(NIPAM-*st*-tBAM)$_{DP}$ nanoparticles obtained with increasing final *DP* of the core-forming P(NIPAM-*st*-tBAM)$_{DP}$ block. For low concentrations (A$_{49}$-*b*-B$_{DP}$LSC): Conventional spherical micelles (**I**) and crew-cut micelles with increasing diameter are formed (**II**&**III**). For high concentrations (A$_{49}$-*b*-B$_{DP}$HSC): Conventional spherical micelles (**IV**), worm-like micelles (**V**) and vesicles (**VI**) are induced. Throughout the report: polymers with the same *DP* are shown with the same background color.

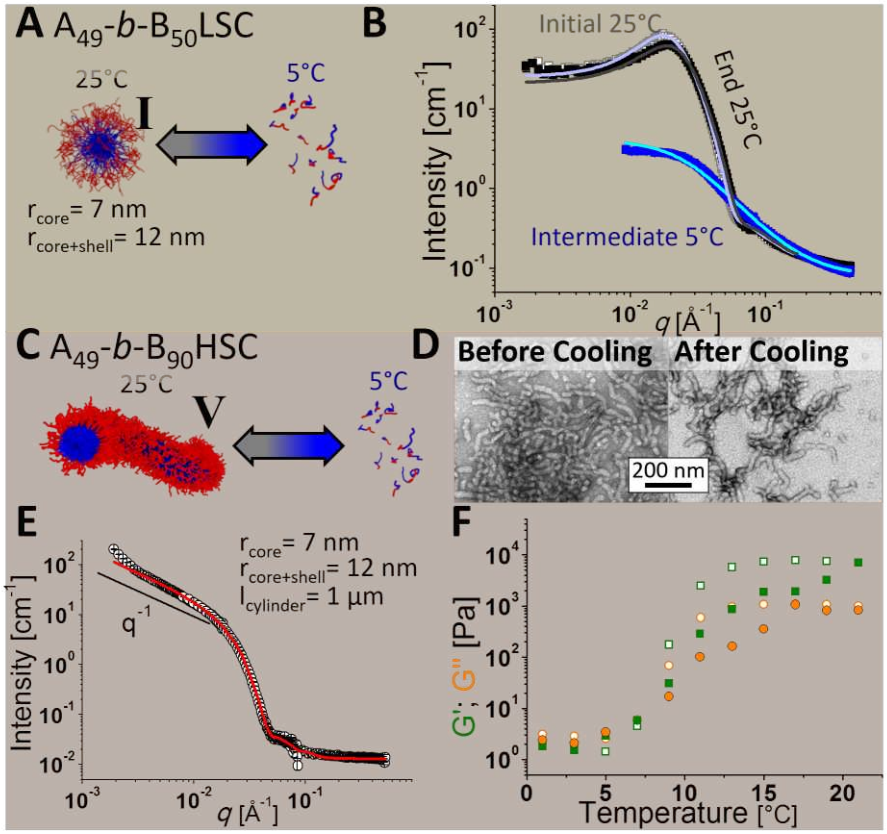

Figure 2. (A) Schematic representation of the thermo-reversible sphere (**I**) to unimer transition observed for A_{49}-*b*-B_{50}LSC. (B) SANS patterns recorded at 25°C (hollow grey symbols; light grey fit line) after cooling to 5 °C (blue symbols; cyan fit line) and on returning to 25°C (solid black symbols; dark grey fit line). Both 25 °C patterns are fit to a spherical core-shell form-factor combined with a structure factor. 5°C sample fits a Gaussian chain form factor.[32] Scattering curves overlap at 25 °C demonstrating reversibility. (C) Schematic representation of a reversible worm (**V**) to unimer transition observed for A_{49}-*b*-B_{90}HSC. (D) TEM before and after a 25°C-5°C-25°C cycle (E) SANS pattern of diluted (A_{49}-*b*-B_{90}HSC) fit to a core-shell cylinder form-factor (red line)[32] (F) Temperature dependent elastic (G' green) and viscous (G" orange) moduli recorded during the temperature cycle (hollow symbols cooling, solid symbols heating). The radius (r) and the length (l) displayed next to the schematic representations is obtained from the fitted SANS data.[32]

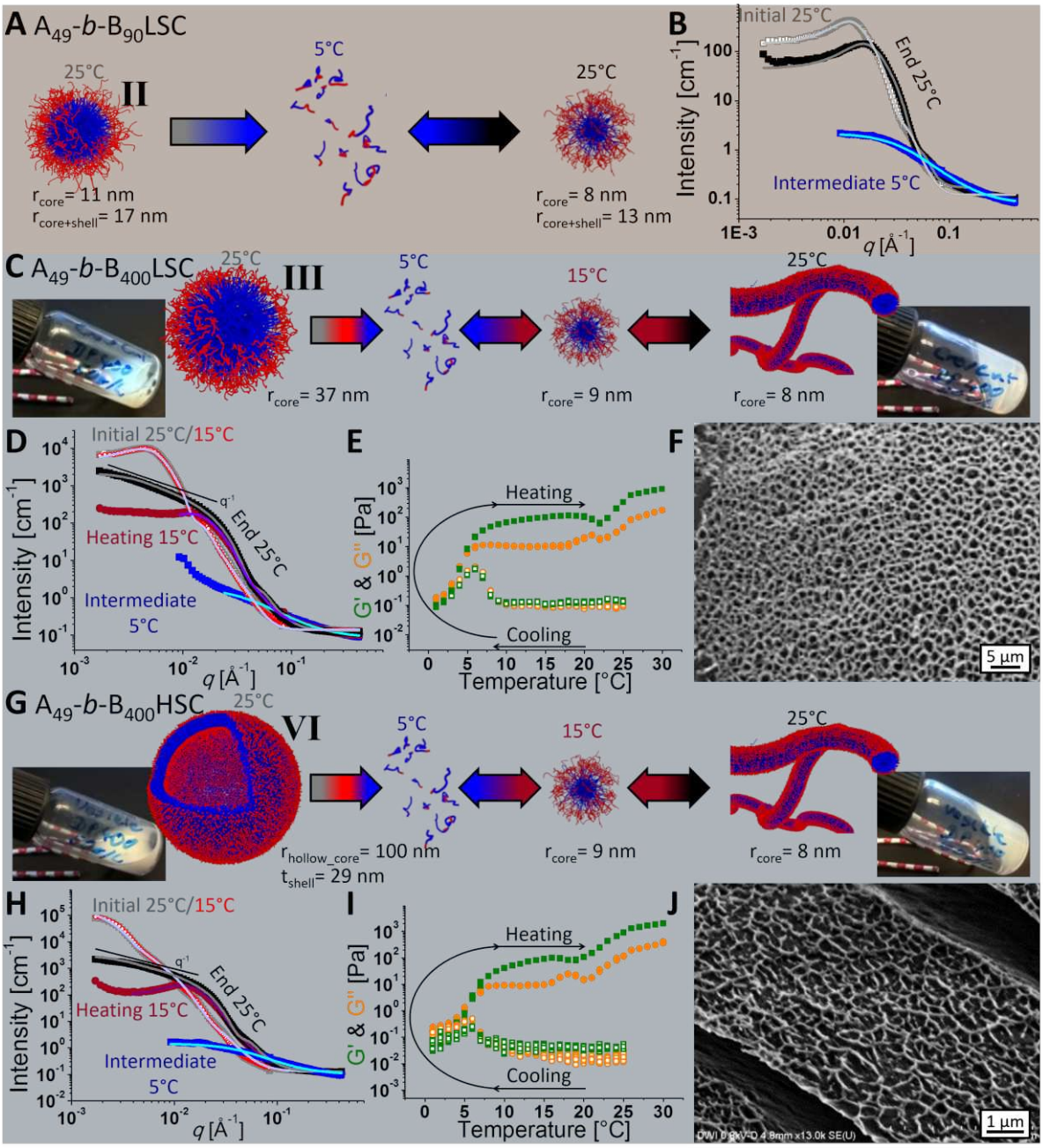

Figure 3. Irreversible micellizations observed after a temperature cycle. (A) Schematic representation of non-equilibrium A_{49}-*b*-B_{90}LSC crew-cut micelle (**II**) dissolution on cooling followed by re-assembly to form smaller spherical micelles (B) Fitted SANS patterns obtained during a temperature cycle conducted on a A_{49}-*b*-B_{90}LSC dispersion of the crew-cut micelles[32] (C) Schematic representation of the morphology changes observed when A_{49}-*b*-B_{400}LSC crew-cut micelles (**III**) experience a temperature cycle; associated digital images show the initial free-flowing dispersion and the final free-standing gel. (D) Fitted SANS patterns[32] and (E) oscillatory rheology data obtained during a temperature cycle conducted on the A_{49}-*b*-B_{400}LSC dispersion. (F) Cryo-SEM image obtained for the A_{49}-*b*-B_{400}LSC gel when returned to 25 °C. (G) Schematic representation of the morphology changes observed when A_{49}-*b*-B_{400}HSC vesicles (**VI**) diluted to LSC experience a temperature cycle; associated digital images showing the initial free-flowing dispersion and the final free-standing gel. (H) Fitted SANS patterns[32] and (I) oscillatory rheology data obtained during a temperature cycle conducted on the diluted A_{49}-*b*-B_{400}HSC dispersion. (J) Cryo-SEM image obtained for the diluted A_{49}-*b*-B_{400}HSC gel on return to 25 °C. SANS data assigned with grey symbols at

25 °C and red symbols at 15°C (before temperature cycle; fitted to spherical core-shell, sphere or hollow sphere models for B, D and H respectively – light grey line), with blue symbols at 5°C (fitted to a Gaussian chain model – cyan line), with dark red symbols at 15 °C (upon heating; fitted to hard sphere model for D and H – purple line) and with black symbols at 25 °C (after temperature cycle; fitted to spherical core-shell for B, cylindrical model for D and H – dark grey line). Rheology data assigned with green symbols for the elastic (G') and orange symbols for the viscous (G") moduli (hollow symbols cooling, solid symbols heating). All measurements at 50 g/L.

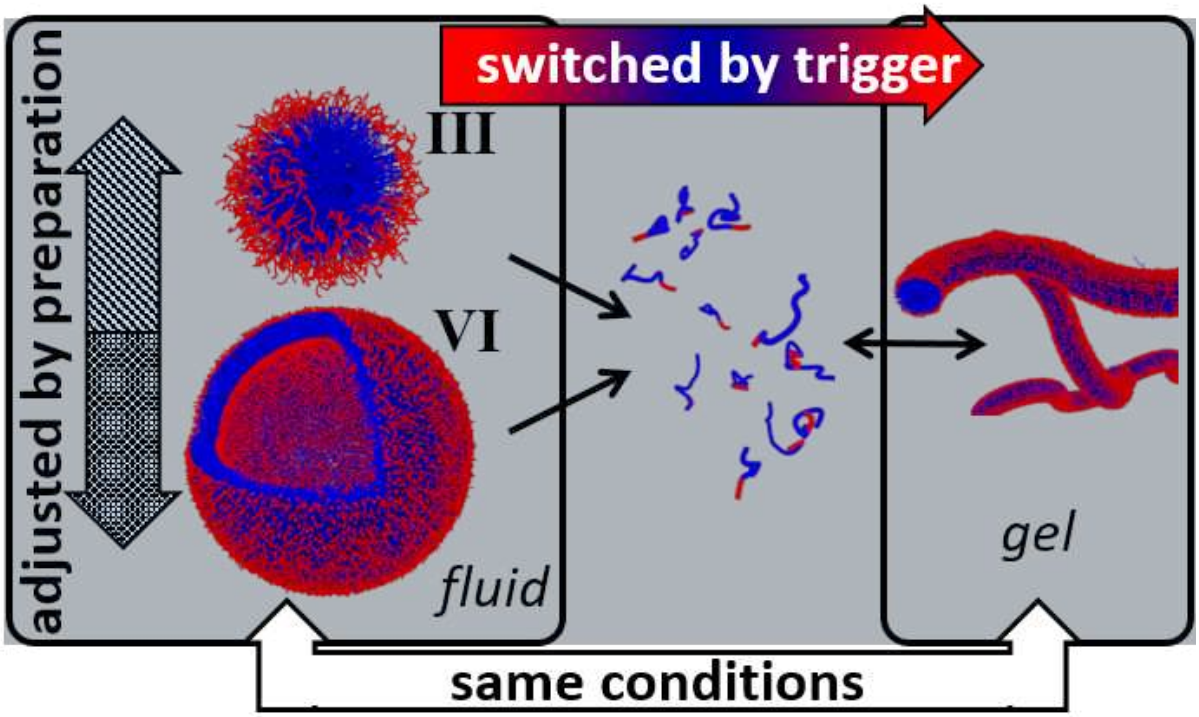

Figure 4. An 'all-morphological' polymer: spherical micelles, vesicles and – after triggering– worm-like micelles are obtained under the same conditions.

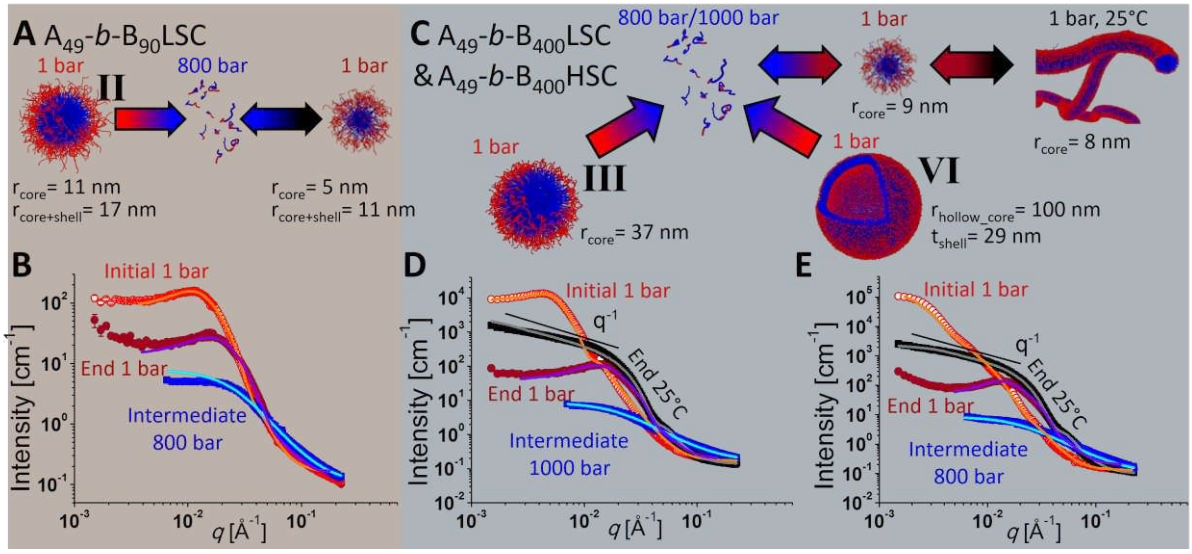

Figure 5. Hydrostatic pressure as stimulus for demicellization and as trigger for irreversible structure changes: (A,B) crew-cut micelle (**II**) to small micelle transition. (C-E) Transition of either crew-cut micelles (**III**) or vesicles (**VI**) to small spheres and subsequently to worm-like micelles. (B) Small crew-cut micelle A_{49}-*b*-B_{90}LSC. (D) Large crew-cut micelle A_{49}-*b*-B_{400}LSC. (E) Vesicle A_{49}-*b*-B_{400}HSC; (B,D,E) SANS data at different pressures (and temperatures) before (hollow symbols) and after pressure trigger (full symbols).[32] 15 °C Ambient pressure before trigger - red (fit orange line), after pressure trigger - dark red (fit purple line). 15 °C 800 bar - blue (1000 bar for A_{49}-*b*-B_{400}LSC, fit cyan line). 25 °C Ambient pressure - black (fit grey line). All measurements at 50 g/L.

The table of contents entry (Short Summary):

Temporary pressure or temperature deflections induce property and morphology changes of easily prepared and kinetically stable non-equilibrium micelles. These systems allow a stimulated physical gelation at constant conditions before and after trigger application. As an extraordinary example, we highlight a specific polymer, which can show all principle micellar morphologies at the same concentration *c*, pressure *p* and temperature *T*.

Keyword micelles, hydrostatic pressure, small angle neutron scattering, rheology, gels

Alexander A. Steinschulte, Andrea Scotti, Khosrow Rahimi, Oleksii Nevskyi, Alex Oppermann, Sabine Schneider, Steffen Bochenek, Marie F. Schulte, Karen Geisel, Felicitas Jansen, Andre Jung, Sabrina Mallmann, Roland Winter, Walter Richtering, Dominik Wöll, Ralf Schweins, Nicholas J. Warren,* Felix A. Plamper*

Stimulated Transitions of Directed Non-Equilibrium Self-Assemblies

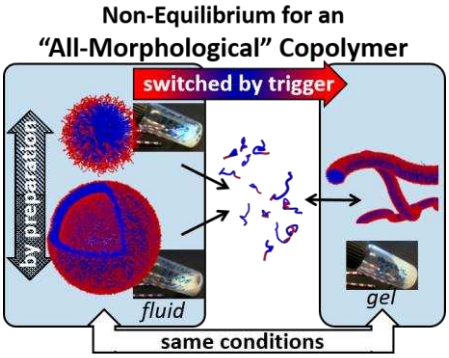

ToC figure